Experimental Study and CFD Simulation of Mass Transfer Characteristics of a Gas-Induced Pulsating Flow Bubble Column

Z. Zhou, Q. Yuan, X. Jia*, W. Feng, and J. Wen

Department of Biological Engineering and Key Laboratory of Systems Bioengineering of the Ministry of Education, School of Chemical Engineering and Technology, Tianjin University, Tianjin 300072, P. R. China

Original scientific paper
Received: May 2, 2012
Accepted: November 2, 2012

Oxygen gas-liquid mass transfer coefficient was measured in a gas-induced pulsating flow bubble column. Pulsating amplitude had a great influence on k_la under pulsating state of equal base flow and pulsating flow, which was enhanced up to 30 % compared with that under steady state; however, it had a negative effect on mass transfer under a fixed low base flow. It was also found that k_la had a negative linear correlation with pulsating frequency. A CFD model considering bubble population balance was applied to simulate the distributions of the gas-liquid interfacial area and the liquid side mass transfer coefficient, finding that the former was in a tight relationship with gas holdup and bubble size distribution, while the latter showed little dependence on fluid flow. Dissolved oxygen (DO) concentrations in liquid phase were predicted, which demonstrated an increasing trend along with time until an almost homogeneous distribution was achieved.

Key words:
Mass transfer, gas-induced pulsating flow, bubble column; mathematical modeling, population balance

Introduction

Gas-liquid two-phase bubble columns have been widely used in various multiphase reactions such as aerobic fermentation and wastewater treatment for their simpler constructions, better defined flow patterns, lower shear fields, better mass transfer capabilities and lower power input in comparison with traditional stirred tanks.[1] Interfacial mass transfer coefficient is an important parameter that affects design and operation of the columns, which is greatly influenced by air flow rate, fluid dynamics (gas holdup, etc.), physical properties (density, viscosity, surface tension, etc.) as well as apparatus geometry.[2,3]

It is known that superimposing fluid pulse in a reactor can improve fluid mechanical conditions and alter flow patterns, achieving an enhanced phase mixing and mass transfer performance.[4,5] The most often investigated devices are trickle bed and pulsed baffled reactor.[4–8] In the former pattern, flow pulse is achieved by natural alteration passage of liquid-rich and gas-rich regions through the bed; while in the latter, there are usually additional baffles fixed in the reactor acting as push fit seal, and furthermore, special energy input devices, e.g. a motor and cam, are also needed to generate a pulsating environment for the system. Krishna and Ellenberger[9] used a loudspeaker to make a liquid vibration in a frequency range of 0–250 Hz; improvement of k_la was achieved by 30–100 %, depending on the operating gas velocities. Knopf et al.[5] studied mass transfer coefficient in a pulsating bubble column at low amplitudes and modest frequencies (0–30 Hz). Godo et al.[10] found that when keeping an airlift reactor in an unsteady state, it was operated more efficiently with increased dissolved oxygen (DO) even under high viscous fermentation.

Under the working conditions mentioned above, pulse was mostly caused by the liquid vibration, which would require special inducing fittings and more energy consumption. In the present work, however, a gas-induced pulsating method was developed to generate a vibration environment in a bubble column, in which gas was introduced into the column through a simply constructed pulse exciter.[11] Local transient fluid flow behaviors of the gas-induced pulsating flow bubble column had been fully investigated with its good performance shown as expected. However, understanding for its mass transfer characteristics was still in blank.

The objective of this work was to, firstly, experimentally investigate the effects of gas-induced pulse on oxygen gas-liquid volumetric mass transfer coefficient in a 24 L rectangular bubble column using the dynamic gassing-out method (GOM), and secondly, to mathematically simulate the distributions of gas-liquid interfacial area, liquid side mass

*Correspondence: Dr. X.Q. Jia (xqjia@tju.edu.cn)

transfer coefficient, as well as DO concentration by developing a computational fluid dynamic (CFD) model with the multiple size group (MUSIG) model implanted, for the first time in application to the specific reactor.

Experiments and methods

Experimental setup and procedures

The experimental apparatus applied in this work was the same as the previous study, as shown in Fig. 1.[11] Distilled water acting as liquid phase was operated under a batch condition with a static

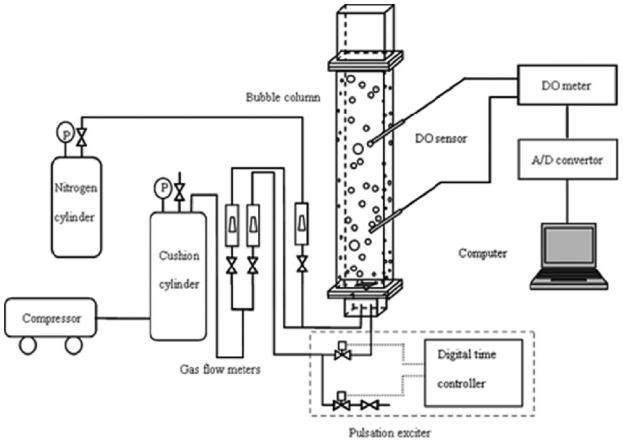

Fig. 1 – *Schematic diagram of the apparatus*

liquid height of 0.6 m. Air was produced by a compressor and then introduced into the column through a square stainless steel perforated plate with a width of 50 mm. The distribution plate contained 625 holes with a diameter of 0.5 mm, which was centrally located at the bottom of the column. Air was divided into two routes, namely, base flow and pulsating flow, each route controlled and measured by a rotor flowmeter. One route acting as the base flow was introduced into the column continuously (0.18 $m^3\ h^{-1}$ to 1.62 $m^3\ h^{-1}$); the other route, the pulsating flow, was regulated by a pulse exciter and then introduced into the column periodically (0.36 $m^3\ h^{-1}$ to 2.88 $m^3\ h^{-1}$).[11] There were two parameters for the characterization of the pulse: pulsating cycle *T*, and pulsating amplitude, consisting of the base flow and the pulsating flow. Pulsating "on" time (opening state) and pulsating "off" time (close state) were all equal to *T/2*. In this manner, a square-wave cycled pulsating gas feed was achieved.[11] Pulsating frequency (*1/T*) was calibrated by counting the pulses for a specified time, which was in a spectrum from 0.5 Hz to 2.67 Hz during the experiments.

Determination of $k_l a$ values

Existing methods for determination of $k_l a$ include the dynamic pressure-step method (DPM), the sulfite oxidation (SOM) and the dynamic gassing-out method (GOM),[12] while the GOM is the most widely applied by many researchers, and also in the current work, although it has certain disadvantages especially for high gas velocities, which was not the case in this work.[4,9,13,14]

First, oxygen was desorbed from the liquid bulk in the bubble column by feeding with pure nitrogen at a flow rate of 0.6 $m^3\ h^{-1}$ for about 15 minutes. After DO concentration in liquid phase reached zero level, the nitrogen flow was shut off and compressed air was fed into the column immediately. Then the time-dependent DO was measured with an oxygen sensor (InPro 6050/120, Mettler-Toledo, Switzerland) connected to a DO meter (O_2 Transmitter 4050e, Mettler-Toledo, Switzerland) at a time interval of 1 s until DO in the liquid bulk almost reached the saturation value. The sensor was placed in the fully developed regime of the reactor, 500 mm from the bottom at a 15° angle to the column, and a lower position, 300 mm from the bottom. The signals from the DO meter were recorded onto a computer though an A/D converter.

Under the assumption of ideal mixing in gas and liquid phases, negligible nitrogen counter-diffusion, constant interfacial area, no significant change of oxygen in gas phase and not considering the effect of the hydrodynamic regime in the vicinity of the sensor compared with the mass transfer dynamics,[12,13] the $k_l a$ values were obtained from the experimental data using the following equation:

$$\frac{c^* - c_L}{c^* - c_0} = \frac{\exp(-k_l a \cdot t) - k_l a \cdot \tau_p \cdot \exp(-t/\tau_p)}{1 - k_l a \cdot \tau_p} \quad (1)$$

where $(c^*\text{-}c_L)$ was the driving force causing oxygen mass transfer from bubbles into liquid bulk; c^* referred to the saturation DO concentration, c_0 the initial value and c_L the time dependent value.

When in the case of using a fast response DO sensor with a low τ_p value, if the $k_l a$ values were also not very large, which satisfied $k_l a \cdot \tau_p < 1$, then Eq. (1) could be rewritten in a simplified form:

$$\frac{c^* - c_L}{c^* - c_0} = \exp(-k_l a \cdot t) \quad (2)$$

Then $k_l a$ was evaluated from the time-dependent DO concentration profiles using a fitting program with the above equation.

The effect of temperature on $k_l a$ should also be taken into consideration for the experiments were carried out under room temperature, which was not

constant all the time. For this purpose, compensated $k_l a$ values were corrected to a standard temperature of 20 °C using the following formula proposed by Whitton and Nienow (1993):[15]

$$k_l a_{20°C} = \frac{k_l a}{1 + 0.02665(T_l - 20)} \tag{3}$$

where T_l was the operating temperature of water in the column, which could also be measured by the sensor simultaneously.

CFD modeling

In this study, a three-dimensional Euler-Euler gas-liquid two-phase CFD model coupling of the MUSIG model considering non-uniform bubble size distribution was developed to simulate the mass transfer characteristics of a gas-induced pulsating flow bubble column. The description of the flow model as well as the details of the MUSIG model including the bubble coalescence and break-up kernels was reported previously,[11] thus was not repeated here.

The two-film theory[16] was adopted to simulate oxygen mass transfer between gas phase and liquid phase. Description of oxygen transport equation was as following:

$$\frac{\partial}{\partial t}(\rho_g \alpha_g x_{o,g}) + \nabla \cdot (\rho_g \alpha_g x_{o,g} \mathbf{u}_g) = \\ = \nabla \cdot \left[\alpha_g \left(\rho_g D_{o,g} + \frac{\mu_{T,g}}{Sc_{T,g}} \right) (\nabla x_{o,g}) \right] - \Gamma_{o,gl} \tag{4}$$

$$\frac{\partial}{\partial t}(\rho_l \alpha_l x_{o,l}) + \nabla \cdot (\rho_l \alpha_l x_{o,l} \mathbf{u}_l) = \\ = \nabla \cdot \left[\alpha_l \left(\rho_l D_{o,l} + \frac{\mu_{T,l}}{Sc_{T,l}} \right) (\nabla x_{o,l}) \right] + \Gamma_{o,gl} \tag{5}$$

The turbulence Schmidt number Sc_T is defined as $Sc_T = \mu_T / \Gamma_T$, where μ_T is the molecular viscosity and Γ_T is the turbulence diffusivity, which has a default value of 0.9.[17]

Nitrogen was considered to be the constraint component in gas phase; water was considered to be the constraint component in liquid phase. Mass fractions of the above two constraint components in corresponding phases were determined by species balance equations:

$$x_{o,g} + x_{n,g} = 1 \tag{6}$$

$$x_{o,l} + x_{n,l} = 1 \tag{7}$$

Gas phase oxygen kinematic diffusivity $D_{o,g} = 2 \times 10^{-5}$ m^2 s^{-1}; liquid phase oxygen kinematic diffusivity $D_{o,l} = 2.54 \times 10^{-9}$ m^2 s^{-1}.[18]

Oxygen inter-phase mass transfer source term was calculated by:

$$\Gamma_{o,gl} = k_l a \alpha_g [(\rho_l x^*_{o,l}) - (\rho_l x_{o,l})] \tag{8}$$

Oxygen gas-liquid mass transfer coefficient was calculated by:[19]

$$k_l = \frac{2}{\sqrt{\pi}} \sqrt{D_{o,l}} \left(\frac{\varepsilon \rho_l}{\mu_l} \right)^{0.25} \tag{9}$$

Liquid phase saturated oxygen mass fraction at the specified gas phase oxygen mass fraction, $x^*_{o,l}$, was calculated through the mass fraction equilibrium ratio of oxygen between the gas-liquid inter-phase.

Gas bubble interfacial area was calculated by:

$$a_g = 6 \alpha_g / d_g \tag{10}$$

Phase density, molecular viscosity, volume fraction, velocity vector, turbulence viscosity, liquid phase turbulence eddy dissipation, and Sauter mean bubble diameter were all obtained from the hydrodynamic CFD model coupling with the MUSIG model presented previously.[11]

Oxygen transport due to gas-liquid inter-phase mass transfer was sufficiently small compared with the main body of each phase, thus its effect on the continuity equations and momentum equations was neglected.[17]

The initial and boundary conditions and the numerical method for solving the developed CFD model in this work were basically the same as the previous study[11], such as $\alpha_g = 1$, $\alpha_l = 0$ for the inlet boundary, degassing condition for the outlet boundary and $\alpha_g = 0$, $\alpha_l = 1$ for the wall boundary (initial state, afterwards calculation determined). Bubble diameter at the distribution plate is assumed to be uniform and was calculated by the correlation presented by Miyahara et al.,[20] which was 4.49 mm. Then the size fraction of the 3rd group of the gas bubbles was set to be 1, whose diameter was 4.5 mm calculated by the equal diameter discretization method.[17] Transient calculations start from assuming that gas volume fraction was 0 in each phase, initial oxygen volume fraction was 0.21 in gas phase and 0 in liquid phase.

Results and discussion

Regression of $k_l a$ values

The equivalent total air flow rate can be calculated by the following equation:

$$Q_{equ} = Q_b + \frac{1}{2} Q_p \tag{11}$$

Then the equivalent superficial gas velocity was obtained from Q_{equ} divided by the bubble column cross-section area:

$$u_g = \frac{Q_{equ}}{S} \tag{12}$$

Correlation between the volumetric mass transfer coefficient and superficial gas velocity was usually represented by an equation of the following type, frequently found in the literature:[3,4]

$$k_l a \propto (u_g)^{\beta} \tag{13}$$

Three different operating conditions were applied in this work respectively: steady state with base flow rate of 0.54 $m^3\ h^{-1}$ to 1.62 $m^3\ h^{-1}$ and without pulsating airflow; pulsating state with a fixed base flow rate of 0.18 $m^3\ h^{-1}$, which was found to be the critical value for this gas-liquid column to be normally fluidized, and pulsating flow rate of 0.72 $m^3\ h^{-1}$ to 2.88 $m^3\ h^{-1}$; pulsating state with equal base flow rate and pulsating flow rate (Q_p=Q_b) of 0.36 $m^3\ h^{-1}$ to 1.08 $m^3\ h^{-1}$. The equivalent superficial gas velocity ranged from 3.75 mm s^{-1} to 11.25 mm s^{-1} in this study.

The regression of $k_l a$ values followed Eq. (2), typical samples were shown in Fig. 2 for two operating states with the same superficial gas velocity. $k_l a$ values obtained in this study ranged from 6×10^{-3} s^{-1} to 15×10^{-3} s^{-1}, while the oxygen probe time constant τ_p was about 6 s of this sensor, indicating that the above assumption of $k_l a \cdot \tau<1$ was justified. It was also found that $k_l a$ obtained from the two different locations of the column almost held the same values within experimental errors. This indicated that the system was in complete mixing state, and the local $k_l a$ measurements can generally represent the overall $k_l a$ of the column. Consequently, only the measured $k_l a$ from the upper location are displayed in this work.

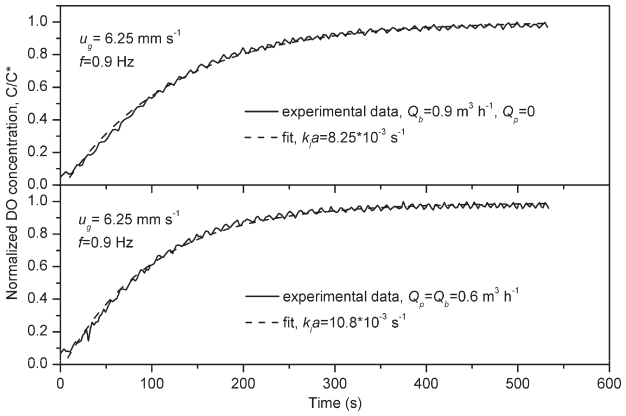

F i g . 2 – *Typical oxygen uptake curves under u_g=0.00625 m s^{-1} and f=0.9 Hz*

Influence of pulsating amplitude on $k_l a$

The pulsating flow rate Q_p was changed to work at different pulsating amplitude, which varied from 0.36 to 2.88 $m^3\ h^{-1}$, and the digital time controller was fixed to t_b=t_p engendering a constant pulsating frequency of 0.9 Hz during the experiments. The experimental observation of the influence of pulsating amplitude on $k_l a$ is shown in Fig. 3. It was noted that $k_l a$ values obtained from the pulsating state with a fixed base flow rate of 0.18 $m^3\ h^{-1}$ were smaller than those obtained from the steady state at the same u_g, and the exponent in Eq. (13) β=0.414 representing the dependence of $k_l a$ on u_g under the pulsating state was also lower than that under the steady state in which β=0.529. This may be due to the equivalent superficial gas velocity comparison necessity for the two different states. For a lower base flow, a higher pulse air influx was required for the balance with the steady state, which would lead to a relatively short contact time between the two phases and thus may limit the mass transfer rate.[6] It can be seen in the experiments that more large bubbles formed in the column as gas flow rate increased; however, many small bubbles were also engendered by the highly induced turbulence. These two-opposite effects may have a great influence on the total interfacial area a, which was a crucial element of the volumetric mass transfer coefficient. Then the compromised pulsating state with equal base flow rate and pulsating flow rate (Q_p=Q_b) was adopted to compensate the abovementioned effects of high air flow rate. As can be seen in Fig. 3, nearly 30 % enhancement in $k_l a$ was achieved under the pulsating state with Q_p=Q_b in comparison with the steady state, especially for higher gas flow rate. The larger exponent β=0.654 was also obtained for this state.

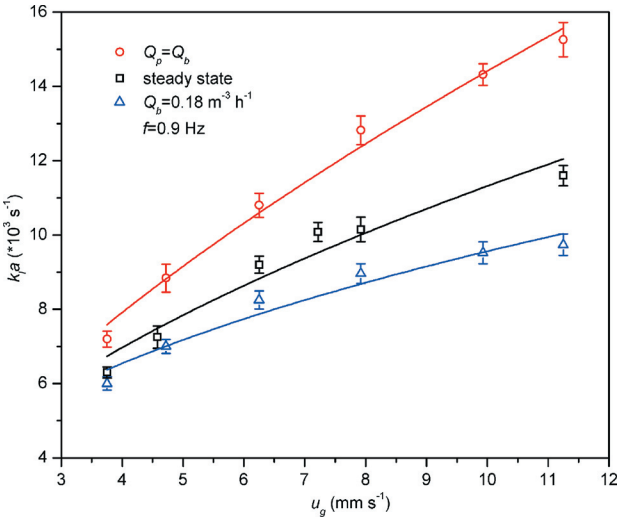

F i g . 3 – *Influence of pulsating amplitude on oxygen volumetric mass transfer coefficient under f=0.9 Hz*

The physical mechanisms responsible for this performance improvement were the highly induced phase turbulence in this air-water non-coalescent system, which would accelerate the recirculation of the induced turbulent liquid flow and the continuous gas-liquid surface renewal by the constant generation and breakup of gas bubbles with phase pulse.

An internal camera CCD bubble measurement technology[21] was applied for the analysis of the local bubble size distribution (BSD) under the different operating conditions. Samples were taken at the upper section of the column. Nearly 300 bubbles of diameters ranging from 1 mm to 15 mm were counted. The circle time averaged BSDs obtained experimentally are shown in Fig. 4. For higher gas flow rate, large fast-rising bubbles or gas caps were observed in the column especially at the lower section. However, the highly developed turbulence would also cause the breakage of large bubbles into small ones. The conjunct performance would have a great influence on the BSDs. As the figure shows, many small bubbles formed under the pulsating state with Q_p=Q_b=0.6 m^3 h^{-1}; while for Q_p=1.44 m^3 h^{-1} and Q_b =0.18 m^3 h^{-1}, a great many large bubbles occupied the column in comparison with the steady state.

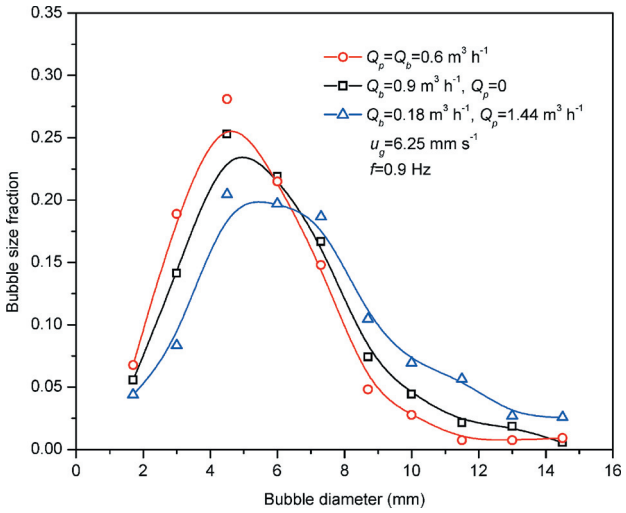

Fig. 4 – *Bubble size distributions for different operating states under u_g=0.00625 m s^{-1} and f=0.9 Hz*

Influence of pulsating frequency on $k_l a$

Different time series with t_b=t_p were used to engender a pulsating frequency spectrum from 0.5 Hz to 2.67 Hz for the unsteady state operations by the time controller. In these experiments, Q_p was kept at a constant value of 1.44 m^3 h^{-1} and Q_b of 0.18 m^3 h^{-1}. The equivalent total air flow rate Q_{equ} as well as the superficial gas velocity u_g were calculated to be the same values with different time series. The increase in frequency f represented the decrease in the pulse feed time t_p and the base feed time t_b, which had a correlation as follows:

$$f = \frac{1}{t_b + t_p} \tag{14}$$

Linear relationship between $k_l a$ and f were found in this study:

$$k_l a \times 10^3 = -1.566 f + 9.438 \tag{15}$$

Linear correlation coefficients R^2 were above 0.99. The minus slope of the curve indicated a decreasing trend of $k_l a$ with the increase in pulsating frequency f for such an operating condition, which is clearly shown in Fig. 5. The decrease in $k_l a$ with the increase in f may be due to the initial bubble size formation at the gas distributor. As can be observed in these experiments, many large bubbles (even some little bubble caps) formed from the distributor at the very beginning of the pulse feed time, which would lead to the decrease in the gas-liquid interfacial area a for the mass transfer process. However, if the pulse flow was fed in continuously as pulse went on, the large bubbles and caps would be replaced by the uniform small bubbles. As a result, $k_l a$ values were higher for lower pulsating frequencies.

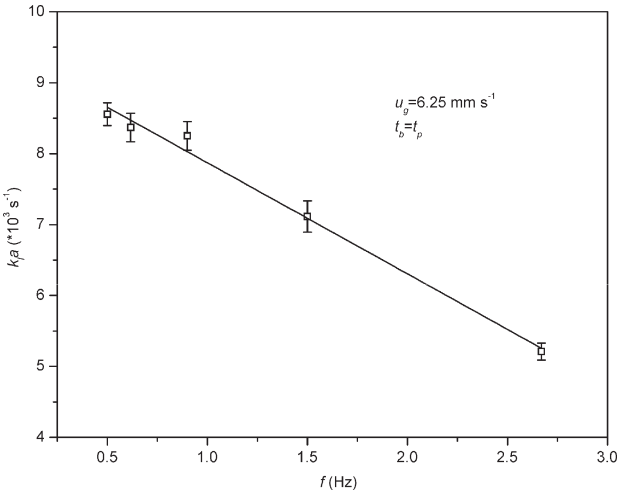

Fig. 5 – *Influence of pulsating frequency on oxygen volumetric mass transfer coefficient under u_g=0.00625 m s^{-1}*

Influence of bubble properties on $k_l a$

Bubble properties, such as size and distribution, have significant effects on oxygen mass transfer in the gas-liquid interface. However, it is expensive and sometimes difficult to experimentally measure the local and transient changes of bubble prop-

erties; therefore, the CFD method may provide us a better alternative.

The distribution of different sized bubbles in the column had been simulated in the previous study.[11] Small bubbles ($d \leq 4.5$ mm) and medium bubbles (4.5 mm $d \leq 7.3$ mm) mainly occupied the bottom and middle regions of the column; while large bubbles ($d > 7.3$ mm) mainly occupied the top and near-wall regions with a low gas holdup.

Bubble properties affected the gas-liquid mass transfer efficiency through interfacial area, a, whose time-dependent fluctuation in the column simulated by the proposed model is shown in Fig. 6 under u_g=0.01 m s^{-1} (Q_p=2.52 m^3 h^{-1} and Q_b=0.18 m^3 h^{-1}) and f=1.25 Hz. It was observed that a periodically fluctuated as a result of gas impulse and bubble swarm's periodic motion, which was intensive in the upper part of the column but gentle in the whole column. The distribution of a corresponded with that of the bubbles, which was larger in the bottom and middle regions of the column, but smaller in the top and near-wall regions. It was also noticed that there were some "dead zones" in the column, especially in the corners of the bottom, which contained very little bubbles, meaning very low oxygen mass transfer efficiency.

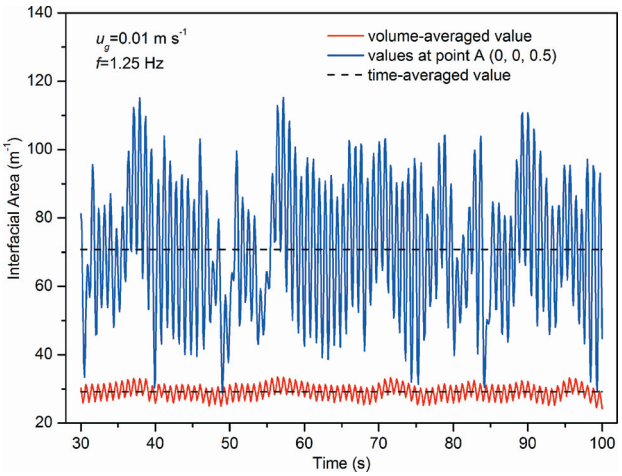

Fig. 6 – *Gas-liquid mass transfer interfacial area fluctuation under u_g=0.01 m s^{-1} (Q_p=2.52 m^3 h^{-1} and Q_b=0.18 m^3 h^{-1}) and f=1.25 Hz*

Fig. 7 was the model prediction of gas holdup, interfacial area and liquid side mass transfer coefficient of the vertical section of the column at two time points. It can be seen that the distribution of a significantly depended on the distribution of gas holdup. However, the distribution of liquid side mass transfer coefficient k_l had a relationship with liquid flow to some extent but changed little in general, whose values ranged from 6×10^{-4} m s^{-1} to 9×10^{-4} m s^{-1}.

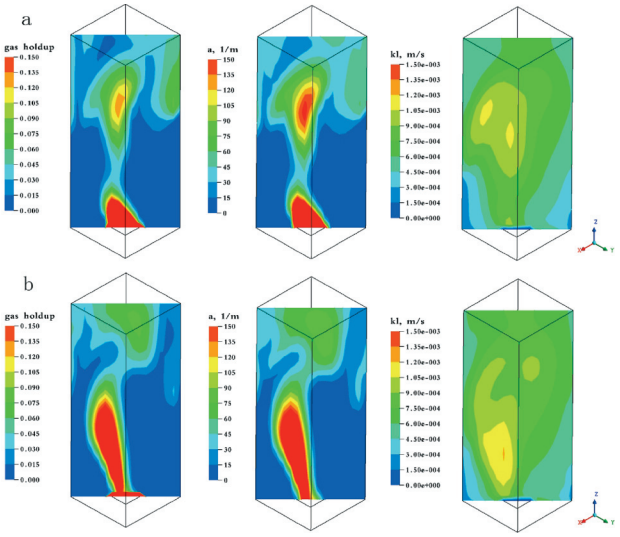

Fig. 7 – *Model prediction of gas holdup, interfacial area and liquid side mass transfer coefficient under u_g=0.01 m s^{-1} (Q_p=2.52 m^3 h^{-1} and Q_b=0.18 m^3 h^{-1}) and f=1.25 Hz (**a**: t=40 s, **b**: t=70 s)*

Model validation of $k_l a$

Fig. 8 was the comparison between model simulated and experiment measured $k_l a$ values under the same operating conditions. Six data points were obtained under u_g=0.01 m s^{-1} (three operating conditions: Q_b=1.44 m^3 h^{-1}, Q_p=2.52 m^3 h^{-1} and Q_b=0.18 m^3 h^{-1}, Q_p=Q_b=0.96 m^3 h^{-1}), f=1.25 Hz and u_g=0.00625 m s^{-1} (three operating conditions: Q_b=0.9 m^3 h^{-1}, Q_p=1.44 m^3 h^{-1} and Q_b=0.18 m^3 h^{-1}, Q_p=Q_b=0.6 m^3 h^{-1}), f=0.9 Hz, respectively. It was noticed that the model simulated values were normally higher than the experimental results, with the maximum error of +30 %. The main reason for the deviation might be that a uniform bubble assump-

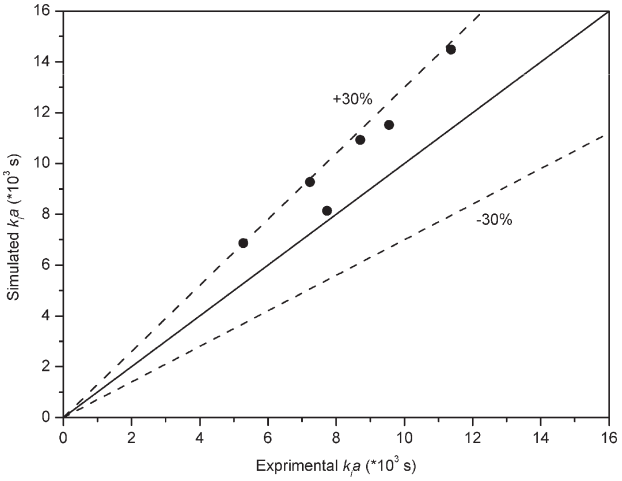

Fig. 8 – *Comparison between experimental and simulated oxygen mass transfer coefficient under u_g=0.01 m s^{-1}, f=1.25 Hz and u_g=0.00625 m s^{-1}, f=0.9 Hz for three different operating conditions, respectively*

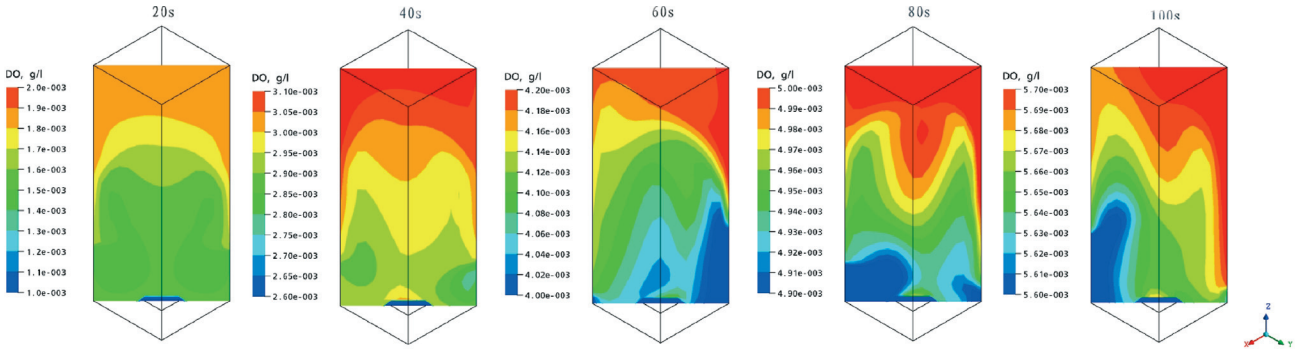

Fig. 9 – *Model prediction of DO distribution under u_g=0.01 m s^{-1} (Q_p=2.52 m^3 h^{-1} and Q_b=0.18 m^3 h^{-1}) and f=1.25 Hz*

tion at the inlet of the column was made in the model, which neglected the effect of the pulsating inlet air and then resulted in a deviation of the model simulated gas distribution.

Prediction of DO distribution

The main advantage for adopting the CFD model in this work was its ability to predict the local and transient mass transfer characteristics of the gas-induced pulsating flow bubble column, for example, the DO concentration distribution in liquid phase within the column, as shown in Fig. 9, to facilitates the understanding and controlling of the corresponding chemical and biochemical processes, which can cover the shortage of the experiments to a large extent.

From this figure, it was observed that DO concentrations increased with time, reaching an almost uniform distribution within the whole column (indicated by the narrowing of the upper and lower limits of the scales). The distribution of DO concentration along the vertical position is also reflected in Fig. 9, whose values increased with height, making the largest ones appear in the top region. This may be mainly attributed to the better mixing of the two phases, as well as a more sufficient mass transfer along with the up-flow gas bubbles and developing fluid flow. However, bubble coalescence had an opposite effect. Larger bubbles had smaller interfacial area which was essential for oxygen mass transfer between phases, thus the top and near-wall regions of the column where larger bubbles accumulated had lower interfacial area compared with the bottom and middle regions of the column where smaller bubbles had accumulated (as shown in Fig. 6), which significantly influences the DO distribution. It was noted that there was a close relationship between the distribution of DO and the fluid flow, which can be concluded by the non-symmetric distribution of dissolved oxygen concentration as the result of the wiggling of the bubble swarms.

DO concentration fluctuations in real bioprocess systems

The most important parameter in real bioprocess systems is definitely the DO concentration, which is essential for aerobic microorganism cultivation. To reveal the DO concentration fluctuations in such systems, new experiments were designed and carried out in a typical bioprocess: phenol biodegradation by *Candida tropicalis* as described by Feng et al.[22] in this specific gas-induced pulsating flow bubble column reactor. Experiments were done in two different cases: Case 1 that started from saturated DO concentration, or Case 2 that started from zero DO concentration in the liquid phase as shown in Fig. 10. Comparisons were made between the simulated reactor volume-averaged DO concentrations calculated by the current model and the experimental data of the averaged value measured by the two DO sensors. Differences were found through the comparisons as the current model did not consider the bioreaction by the biomass (*Candida tropicalis*) and the substrates (phenol and oxygen). In Case 1, the decrease in the DO concentration as a result of biomass consumption was captured experimentally but was ignored in model sim-

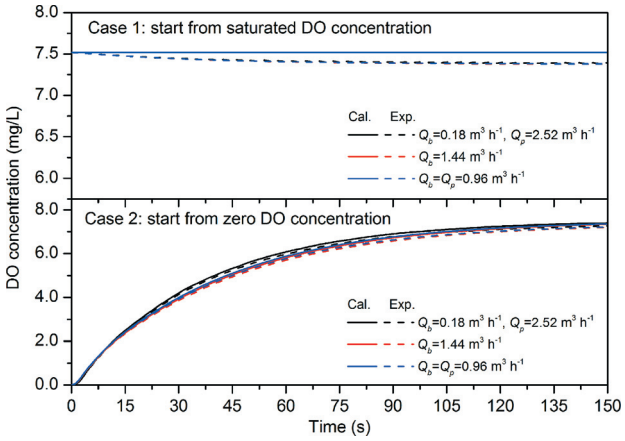

Fig. 10 – *Model prediction and experimental measurement of DO concentration fluctuations under u_g=0.01 m s^{-1} (Q_p=2.52 m^3 h^{-1} and Q_b=0.18 m^3 h^{-1}) and f=1.25 Hz*

ulations, which only hold a constant value. In Case 2, the increase in the DO concentration was both noticed in experiments as well as simulations. Because the oxygen bioreaction consumption rate was much smaller than the mass transfer rate, the difference between the experimental data and model predictions was not so obvious compared with Case 1. Moreover, it could be confirmed in these experiments that the pulsating state flow with the fixed base flow rate of Q_b=0.18 m^3 h^{-1} and the pulsating flow rate of Q_p=2.52 m^3 h^{-1} did have an advantage in oxygen supply in the liquid phase in such a short time (150 s) compared with the steady state flow with the base flow rate of Q_b=1.44 m^3 h^{-1} and the pulsating state flow with equal base flow rate and pulsating flow rate of Q_b=Q_b=0.96 m^3 h^{-1} under the same superficial gas velocity u=0.01 m s^{-1} and pulsating frequency of f=1.25 Hz in real bioprocess systems.

Conclusions

In this study, gas-liquid mass transfer characteristics in a gas-induced pulsating flow square cross-sectioned bubble column was investigated for the first time by both experimental measurement and model simulation.

The effects of pulsating amplitude and frequency on k_la were investigated experimentally, and the bubble size distributions are given for different air influx feedings with the same superficial gas velocity u_g. It was found that there was a notable difference in the volumetric mass transfer coefficient subjected to the steady and pulsating flows, which indicated the advantage for the adoption of the gas pulse operation. It was concluded that enhancement of k_la could be achieved for the synchronized change of base flow as well as pulsating flow (Q_p=Q_b) with the same u_g in comparison with the steady state, especially under high u_g. Moreover, k_la in the gas-induced pulsating flow bubble column was found to be in negative linear correlation with pulsating frequency.

In the hope of gaining more detailed insight into the mechanism of such an unsteady pulsating operation, a three-dimensional CFD model coupling of the MUSIG model considering bubble size distribution was developed to simulate the distribution of the strongly flow-dependent parameters, like interfacial area and liquid side mass transfer coefficient, which was surely to be a necessary and important supplement to experimental technologies. Furthermore, information of local and transient mass transfer properties, such as dissolved oxygen in liquid phase, was also predicted by the proposed model, giving a direct visualization of its distribution along with time and different location within the column. Comparison between measured and simulated k_la was done to validate the model. Errors occurred but lied within a reasonable and acceptable range, which may be improved by better modeling strategies in future work. DO concentration fluctuations in a real bioprocess system, phenol biodegradation by *Candida tropicalis*, were experimentally investigated and the advantage of the gas-induced pulsating flow in supply of oxygen in the liquid phase was confirmed.

ACKNOWLEDGEMENTS

This work was financially supported by the National Natural Science Foundation of China (No. 20906070) and the Seed Foundation of Tianjin University.

Symbols

a – interfacial area, m^{-1}
c – DO concentration, kg m^{-3}
c_L – time dependent DO concentration, kg m^{-3}
D – kinematic diffusivity, m^2 s^{-1}
d – diameter, m
f – pulsating frequency, Hz
k_l – liquid side mass transfer coefficient, m s^{-1}
k_la – volumetric mass transfer coefficient, s^{-1}
$k_la_{20°C}$ – volumetric mass transfer coefficient at 20 °C, s^{-1}
Q – air flow rate, m^3 h^{-1}
S – bubble column cross-section area, m^2
Sc_T – turbulence Schmidt number, defined as Sc_T=μ_T/Γ_T, default value of 0.9
T – pulsating cycle, s
T_l – operating water temperature, °C
t – time, s
u_g – equivalent superficial gas velocity, m s^{-1}
u – velocity vector, m s^{-1}
x – mass fraction

Greek letters

α – holdup
β – constant
Γ – mass transfer source term, kg m^{-3} s^{-1}
ε – turbulence eddy dissipation, m^2 s^{-3}
μ – molecular viscosity, Pa s
ρ – density, kg m^{-3}
τ_p – oxygen probe time constant, s

Superscript

* – saturation state

Subscripts

0 – initial state
b – base state
equ – equivalent state
G – gas phase
inlet – inlet
l – liquid phase
n – nitrogen
o – oxygen
p – pulsating state
T – turbulence
w – water

References

1. *Kaštánek, F., Sharp, D. H.,* Chemical reactors for gas-liquid systems, pp. 330–344, Ellis Horwood, Chichester, UK, 1993
2. *Camarasa, E., Vial, C., Poncin, S., wild, G., Midoux, N., Bouillard, J.,* Chem. Eng. Process. **38** (1999) 329.
3. *Ozbek, B., Gayik, S.,* Process Biochem. **38** (2001) 729.
4. *Ni, X. W., Gao, S. W.,* J. Chem. Technol. Biotechnol. **65** (1996) 65.
5. *Knopf, F. C., Ma, J., Rice, R. G., Nikitopoulos, D.,* AIChE J. **52** (2006) 1103.
6. *Boelhouwer, J. G., Pieoers, H. W., Drinkenburg, A. A. H.,* Chem. Eng. Sci. **54** (1999) 4661.
7. *Oliveira, M. S. N., Ni, X.,* Chem. Eng. Sci. **56** (2001) 6143.
8. *Banchero, M., Manna, L., Sicardi, S., Boelhouwer, J. G., Urseanu, M. I., Kwant, G.,* Chem. Eng. Sci. **59** (2004) 5411.
9. *Krishna, R., Ellenberger, J.,* Chem. Eng. Technol. **25** (2002) 159.
10. *Godo, S., Klein, J., Polakovic, M., Bales, V.,* Chem. Eng. Sci. **54** (1999) 4937.
11. *Jia, X. Q., Yuan, Q., Wen, J. P., Feng, W.,* Chem. Biochem. Eng. Q. **25** (2011) 27.
12. *Blazej, M., Jurascik, M., Annus, J., Markos, J.,* J. Chem. Technol. Biotechnol. **79** (2004) 1405.
13. *Wen, J. P., Na, P., Huang, L., Chen, Y. L.,* Biochem. Eng. J. **5** (2000) 225.
14. *Gourich, B., Vial, C., El Azher, N., Soulami, M. B., Ziyad, M.,* Chem. Eng. Sci. **61** (2006) 6218.
15. *Whitton, M. J., Nienow, A. W.,* 3rd International Conference on Bioreactor and Bioprocess Fluid Dynamics (1993) 135.
16. *Lewis, W. K., Withman, W. G.,* Ind. Eng. Chem. **16** (1924) 1215.
17. *ANSYS Canada Ltd.* ANSYS CFX-Solver, Release 10.0: Theory, Waterloo, Canada, 2005.
18. *Washburn, E. W.,* International Critical Tables, pp. 255–261, McGraw-Hill, New York, 1926.
19. *Dhanasekharan, K. M., Sanyal, J., Jain, A., Haidari, A.,* Chem. Eng. Sci. **60** (2005) 213.
20. *Miyahara, T., Matsuba, Y., Takahashi, T.*, Int. Chem. Eng. **23** (1983) 517.
21. *Feng, W., Wen, J. P., Fan, J. H., Yuan, Q., Jia, X. Q., Sun, Y.,* Chem. Eng. Sci. **60** (2005) 6887.
22. *Feng, W., Wen. J. P., Jia, X. Q., Yuan, Q., Sun, Y., Liu C. Y.,* AIChE J. **52** (2006) 2864.